INFLOW AND FATIGUE RESPONSE OF THE NWTC ADVANCED RESEARCH TURBINE*†

Herbert J. Sutherland
Wind Energy Technology Department
Sandia National Laboratory
Albuquerque, NM 87185-0708
hjsuthe@sandia.gov

Neil D. Kelley
M. Maureen Hand
NREL/National Wind Technology Center
Golden, CO 80401
neil_kelley@nrel.gov, maureen_hand@nrel.gov

ABSTRACT

The Long-term Inflow and Structural Test (LIST) program is collecting long-term inflow and structural response data to characterize the spectrum of loads on wind turbines. In one of the measurement campaigns being conducted under this program, the 42-m diameter, 600-kW NWTC Advanced Research Turbine (ART) was monitored. The inflow was monitored with a planar array of five high-resolution sonic anemometers and supporting meteorological instrumentation located 1.5 diameters upwind of the turbine. The structural response of the turbine was measured using strain gauges circuits and an inertial measurement unit (IMU). The former was used to monitor root bending moments and the low-speed shaft torque, while the latter were used to monitor the motion of the tower and the nacelle. Auxiliary gauges measured blade pitch, rotor teeter, nacelle yaw and generator power. A total of 3299 10-minute records were collected for analysis. From this set, 1044 records are used to examine the influence of various inflow parameters on fatigue loads. Long-term fatigue loads and extreme loads are also examined.

INTRODUCTION

One of the objectives of the Long-term Inflow and Structural Test (LIST) was to develop a physical understanding of the influence of inflow turbulence on the structural response of wind turbines. This requires detailed inflow and turbine measurements over a long time period, a complete wind season for instance. One of the sites instrumented for this project is at the National Renewable Energy Laboratory's National Wind Technology Center near Boulder, Colorado. A 600 kW, 42-m diameter wind turbine was used for this purpose for one typical wind season, October, 2000 to May, 2001. A 42-m diameter planar array consisting of five high-resolution ultrasonic anemometers and supporting meteorological instrumentation was installed 1.5 diameters in the predominately upwind direction of the turbine. A number of aeroelastic, structural, and supporting measurements were made on the wind turbine. A total of 1568 10-minute records were collected where the turbine operated throughout the duration of the record and the mean wind direction remained within ±45°of the perpendicular to the planar array.

Using these data, several analyses are conducted here. The first is an investigation of the correlation of the various (15) inflow parameters on fatigue loads. The second is a comparison of relatively long term fatigue spectra to short term spectra. And, finally, an examination of extreme loads based on the extreme from each 10-minute data set. For each of these analyses, the data records are segregated by their mean wind speed into wind speed classes 5 through 9. For this paper, these classes are defined to be 9-to11, 11-to 13, 13-to-15, 15-to-17, and greater than 17 m/s, respectively.

*This work is supported by the U.S. Department of Energy under Contract DE-AC04-94AL85000 and DE-AC36-83CH10093. Sandia is a multiprogram laboratory operated by Sandia Corporation, a Lockheed Martin company. A portion of the work was performed by the National Renewable Energy Laboratory in support of the U.S. Department of Energy under contract number DE-AC36-99-GO10337.

Fig. 1. NWTC LIST 42-m Inflow Measurement Array Upwind of ART Turbine and Looking Towards Prevailing Wind Direction.

EXPERIMENTAL OVERVIEW

The Advanced Research Turbine (ART, previously known as ART-1) used in this measurement campaign is a Westinghouse 600-kW wind turbine [1] that is currently located at the National Wind Technology Center (NWTC) near Boulder, Colorado. The turbine was initially located on the north shore of the island of Oahu, Hawaii where its initial dynamic response was measured by Snow, et al. [1] and Hock et al. [2]. The turbine was later moved to the NWTC and refurbished for continued operation in its original configuration. Numerical modeling studies [3], [4] used turbine measurements from the new site for model validation. Under the auspices of the LIST program, Kelley et al [5] installed the planar array 1.5 diameters upwind of the turbine and collected a long-term data set that includes both the dynamic response of the turbine and detailed inflow measurements. Only the latter data set is analyzed here.

Turbine Measurements

The Westinghouse 600-kW wind turbine [1] is an upwind, two-bladed teetered-hub machine. It has full span pitch control and a synchronous generator, see Fig. 1. The turbine has a rotor diameter of 42 m (137.8 ft.) and a hub height of 36.6 m (120 ft). The turbine is a constant speed machine (43 rpm) that reaches rated power at 12.8 m/s (28.6 mph). Its cut-in wind speed is 6.25 m/s (14 mph) and its cut-out wind speed is 22.3 m/s (50 mph). In order to maintain turbine operation at higher wind speeds, the pitch control system was adjusted to marginally increase the cut-out wind speed mid-way through the wind season.

The turbine blades are constructed from a wood/epoxy laminate. They have a modified LS(1)-04XX airfoil with a nonlinear, 6.75° twist and no pre-cone angle. Their first (cantilever) bending frequency is 2.24 Hz in the flapwise direction and 4.56 Hz in the edgewise direction. The hub is mounted at a tilt angle of 4°.

The turbine was instrumented to capture the dynamic response of the operating wind turbine to the influence of the inflow turbulence [5]. Strain gauges were used to measure flapwise and edgewise root-bending moments on each blade as well as low-speed shaft torque. The state measurements on the turbine included rotor azimuth position, teeter angle, blade pitch angle, and yaw angle that were obtained with absolute digital position encoders. The generator power was also recorded. An inertial measurement unit (IMU) consisting of an orthogonal triad of ±2g force-balance accelerometers and three ±100 deg/s rate gyroscopes was mounted on the forward low-speed shaft support bearing housing immediately behind the rotor. This paper deals with the root bending moment measurements.

The dynamic response of the turbine is recorded as time series that are divided into 10-minute segments. The flapwise and edgewise root bending gauge signals contained in these histograms are the primary response parameters analyzed here. The initial 50 seconds of the bending signals from a typical time series are shown in Fig. 2.

Inflow Measurements

The inflow instrumentation was mounted on three towers located 1.5–rotor diameters upstream of the turbine rotor. A total of five high-resolution ultrasonic anemometers/thermometers were deployed. In addition, cup anemometers and wind vanes were installed on the central tower at three levels, along with air temperature, fast-response temperature, temperature difference between 3 and 61 m, and dew point temperature sensors. Barometric pressure was

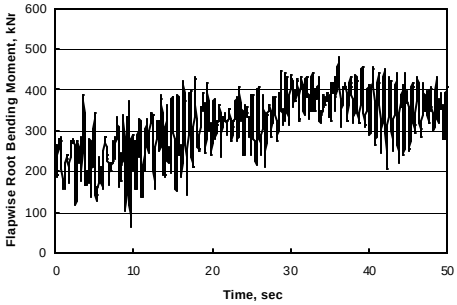

Fig. 2a. Flapwise Bending in the Blade Root.

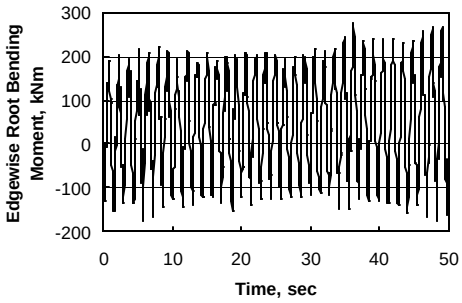

Fig. 2b. Edgewise Bending in the Blade Root.

Fig. 2. Typical Blade Root Time Series for a Mean Wind Speed of 14.0 m/s.

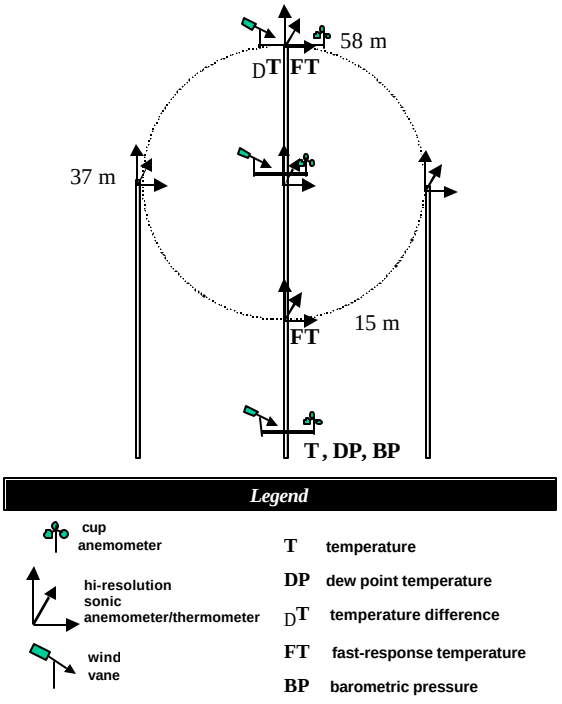

Fig 3. Schematic of NWTC LIST Inflow Measurement Array Instrumentation Deployment.

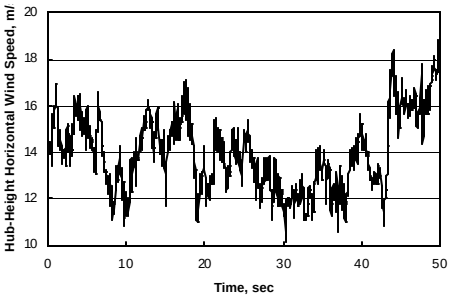

Fig. 4a. Hub-Height Horizontal Wind Speed.

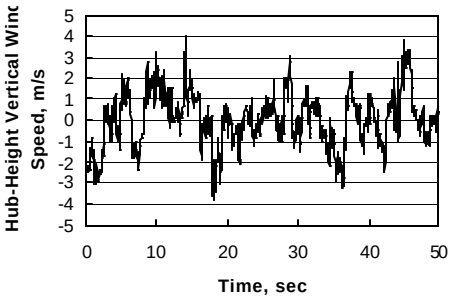

Fig. 4b. Hub-Height Vertical Wind Speed.

Fig. 4. Typical Wind Speed Time Series from the Planar Array of Sonic Anemometers.

measured at a height of 3 m. A schematic of the inflow measurement array is shown in Fig. 3. The inflow parameters discussed in this paper rely on hub-height sonic anemometer wind measurements and central tower temperature and vertical wind shear measurements.

Data System

The inflow and turbine-based data systems were synchronized using a Global Positioning System (GPS) satellite-based time signal. The inflow system sampled at 40 Hz yielding a Nyquist frequency of 20 Hz. The turbine data system sampled at 512.8 Hz and used 20 Hz, six-pole, low-pass Butterworth filters on all analog channels. The data was decimated to 40 Hz for merging with the inflow signals. Further detail may be found in Kelley et al. [5].

Typical time series of the hub-height horizontal and vertical wind speeds are shown in Fig. 4. These records correspond to the bending moment time histories shown in Fig. 2.

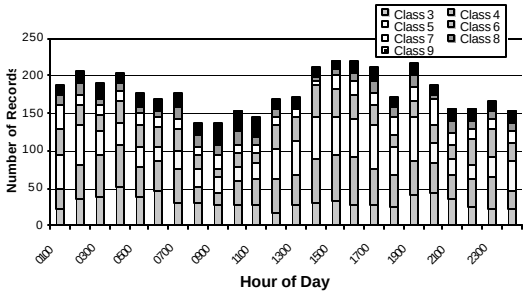

Fig. 5a. All Inflow Records.

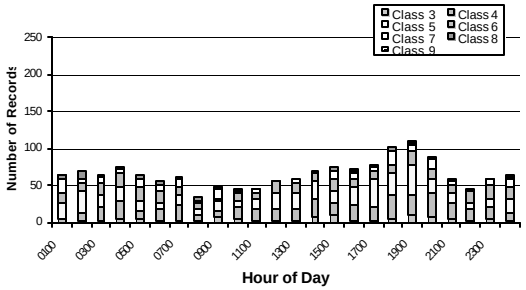

Fig. 5b. Records During Turbine Operation.

Fig. 5. Diurnal variation of wind speed for available inflow (top) and turbine operation conditions (bottom).

THE DATA SET

A total of 1568 10-minute records were collected where the turbine operated throughout the duration of the record, and the mean wind direction remained within ±45º of the perpendicular to the planar array. These records were binned by hub-height mean wind speed into bins of 2 m/s. The diurnal distribution of these records by wind speed class is shown in Fig. 5. The subsequent analyses examine wind speed classes 5 through 9: 9-to-11, 11-to-13, 13-to-15, 15-to-17, and greater than 17 m/s. The number of records contained in each bin is 445, 326, 195, 71 and 7, respectively, see Fig. 6. The diurnal distribution of the wind speed classes for the periods when the turbine was operating is shown in Fig. 5a. For comparison, the diurnal variation of the wind speed classes obtained from the upwind planar array is shown in Fig. 5b. The differences illustrate the periods where the turbine was not in operation due to wind conditions outside its operating range or was otherwise unavailable.

Turbine Response

For completeness, the dynamic response of the turbine is included in this manuscript. Hock et al. [2], McCoy et al. [3], and Malcolm et al. [44] present similar data.

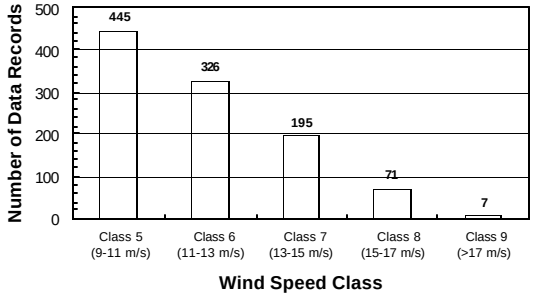

Fig. 6. Distribution of Data Records by Wind Speed Class.

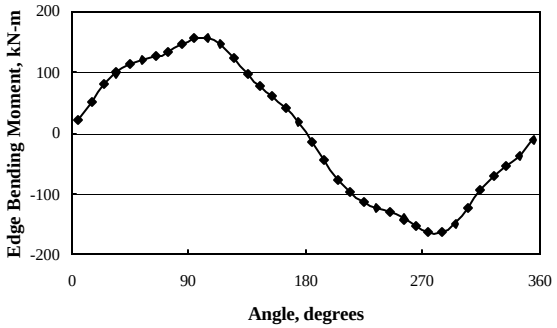

Fig. 7. Azimuth-Averaged Edgewise Bending Moment at a Mean Wind Speed of 14.0 m/s.

Edgewise Bending Moment

The azimuth-averaged edgewise bending moment for root bending, over a 10-minute period, is shown in Fig. 7.

Power Spectral Density

The power spectral density (PSD) plots for the root bending moments are shown in Fig. 8. As shown in this figure, the primary bending moment harmonic in both the edge and flap directions occurs at the system rotation rate, 1P, of 0.72 Hz (43 rpm). For flapwise bending, the even multiples of rotation rate 2P and 4P have major spikes in the PSD curve, see Fig. 5a. For edgewise bending, a 2P spike is present, and the odd multiples 3P and 5p have major spikes in the PSD curve, see Fig. 5b.

Fatigue Spectra

Typical fatigue spectra, obtained by rainflow counting the time series data, are shown in Fig. 9. The spectra were obtained by concatenating the 7 10-minute bending moment time series for Class 9 wind speeds and rainflow counting them. In the counting process, all

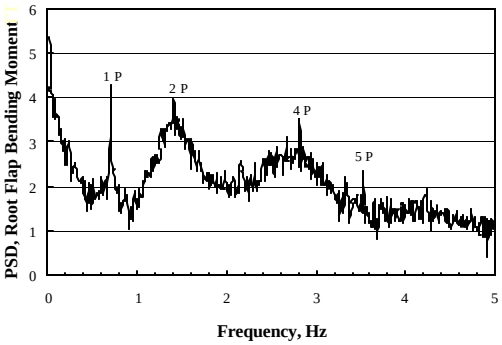

Fig. 8a. Flapwise Bending Moment at the Blade Root.

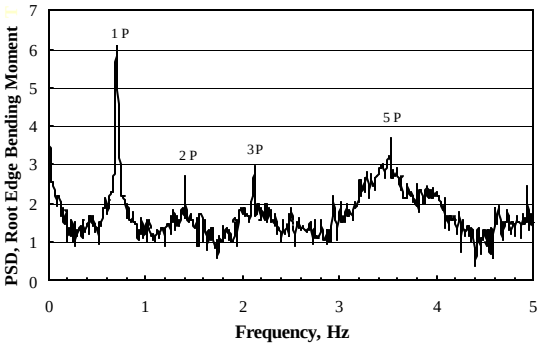

Fig. 8b. Edgewise Bending Moment at the Blade Root.

Fig. 8. PSD for Root Bending at a Mean Wind Speed of 14.0 m/s.

cycles are closed and "half-cycles" are counted whole cycles.

In the spectra presented in Fig. 9, many of the highest bins contain only 1 cycle count. This so-called "floor" occurs at approximately 1 cycle counts per hour for the nominal 1-hour data set. This floor is easily observed in the data presented in Fig. 9a and 9b in bins above approximately 400 kNm and 450 kNm, respectively. The importance of the floor is that it defines the region of the spectra where the data are not statistically significant.

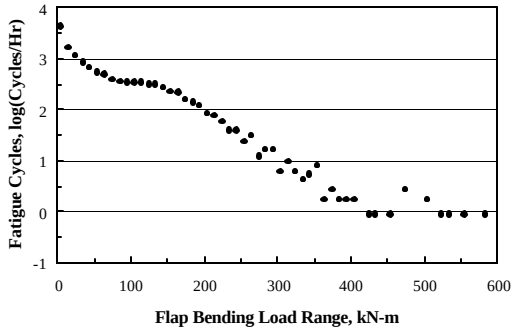

Fig. 9a. Flatwise Bending Moment.

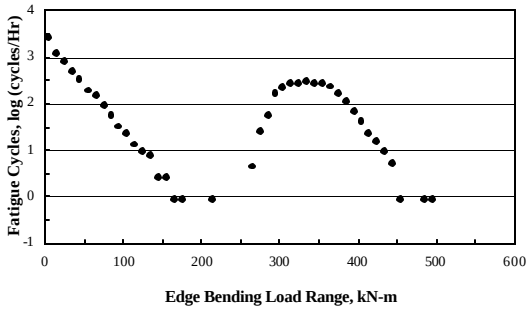

Fig. 9b. Edgewise Bending Moment.

Fig. 9. Typical Fatigue Spectra for Root Bending Moments, Class 9 Wind Speed.

For the correlation analysis, the flapwise and edgewise bending spectra from each 10-minute time history are characterized using the equivalent fatigue load [6,7,8, 9]. For this study, the load is determined using three fatigue exponents, 3, 6 and 10. These values correspond to welded steel, extruded aluminum and fiberglass composite materials, respectively.

Inflow Characterization

Over the past few years, many inflow parameters have been proposed as having influence over the fatigue loads on a wind turbine. The mean wind speed and turbulence (or turbulence intensity) are the most widely recognized as having the major influence on loads. Additional proposed parameters have been summarized to a large extent by Rohatgi and Nelson [10], Fragoulis [6] and Glinou and Fragoulis [7], and Kelley [11, 12, 13].

Fifteen (15) of these secondary parameters are examined here. They are: (1) the standard deviation of the cross-rotor component of the inflow wind speed, $s(v')$; (2) the standard deviation of the vertical component of the inflow wind speed, $s(w')$; (3) the skewness of the horizontal component of the inflow wind speed, U_S; (4) the normalized kurtosis of the horizontal component of the inflow wind speed, U_K; (5) the turbulence kinetic energy, *TKE*; (6) the gradient Richardson number, *Ri*; (7) the vertical wind shear exponent over the rotor, *a*; (8) the local stability

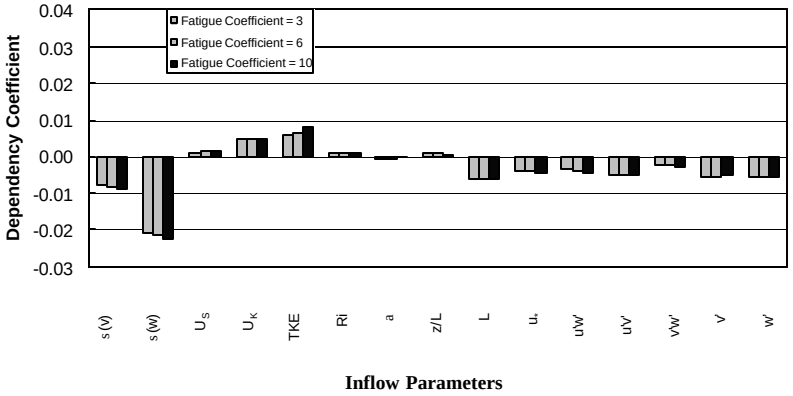

Fig. 10a. Flapwise Bending.

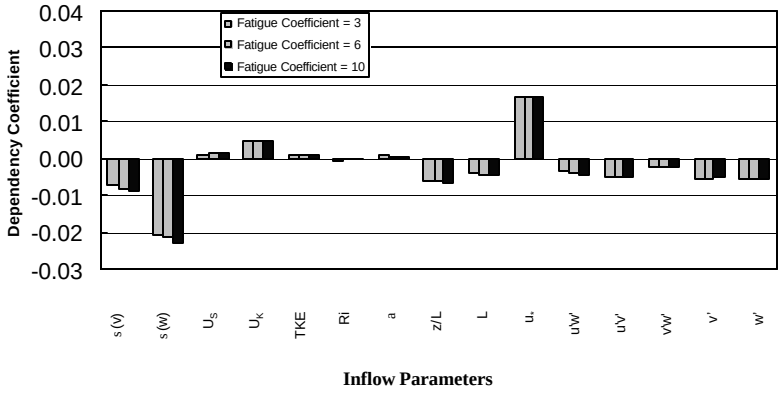

Fig. 10b. Edgewise Bending.

Fig. 10. Dependence Coefficients for Class 6 Wind Speeds.

parameter, *z/L*; (9) the hub-height Obukhov scaling length, *L*; (10) the local friction velocity, u_*; (11, 12, 13) the mean Reynolds stresses *u'w'*, *u'v'* and *v'w'*; (14) the mean cross-rotor turbulent eddy component xxxx; (15) the mean vertical turbulent eddy component *w'*.

These parameters are described in detail in the cited references and the Appendix. However, the thermodynamic parameters, such as the gradient Richardson number, deserve a special explanation, because they are important in understanding the evolution of the turbulence. The gradient Richardson number represents the ratio of turbulence generation or damping by buoyancy (thermal) to wind shear (mechanical) forces. Negative numbers represent *unstable* flow conditions where turbulence is being generated thermally (positive buoyancy) as well as by wind shear. An *Ri* value of zero represents *neutral* conditions in which turbulence generation is taking place solely by mechanical means through the action of wind shear. Positive *Ri* values indicate the presence of *stable* flow conditions in which buoyancy forces act to damp turbulence being generated by wind shear. Positive values of *Ri* represent turbulence that is being generated mechanically by wind shear but is being *damped* by buoyancy forces. Turbulence generated in *critically stable* flows ($0 < Ri < 0.25$) can support the generation of non-linear flow phenomena such as various forms of short-period atmospheric wave motions and shear instabilities which are responsible for bursts of turbulence.

CORRELATION OF INFLOW PARAMETERS

The correlation of the inflow parameters to the structural response of the turbine is examined here using a linear, multi-variable regression to relate the 15 inflow parameters to the equivalent fatigue load. The "dependence coefficient" [6,8] is used to quantify the influence of each inflow parameter on the fatigue loads.

For this analysis, the data are divided into multiple bins based on their mean hub-height wind speed. Wind speed classes 5 through 9 are examined here.

Previous Studies

Several other researchers have investigated the effect of inflow turbulence on the structural response of wind turbines. Three such investigations conducted by Kelley [13], by Fragoulis [6] and Glinou and Fragoulis [7], and by Sutherland [8,9] have examined the influence of various inflow parameters on equivalent fatigue loads. These investigations studied various inflow environments; namely, multi-row wind parks, near complex terrain, and in smooth terrain, respectively.

Kelley [13] used linear multi-variable regression analysis and Analysis of Variance (ANOVA)

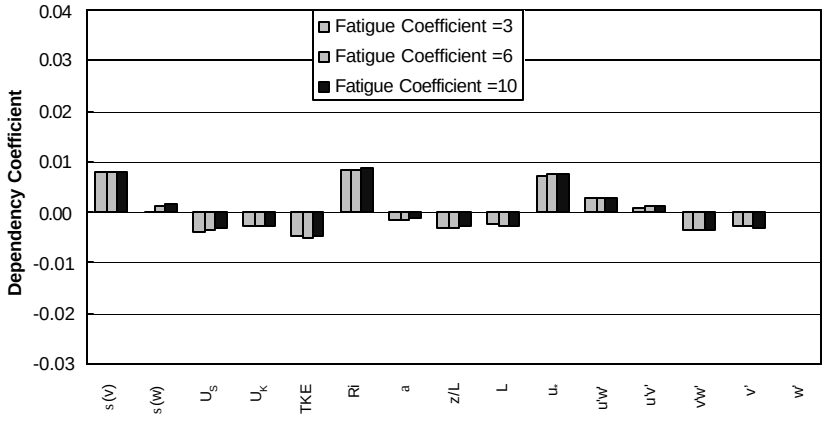

Fig. 11a. Wind Speed Class 5.

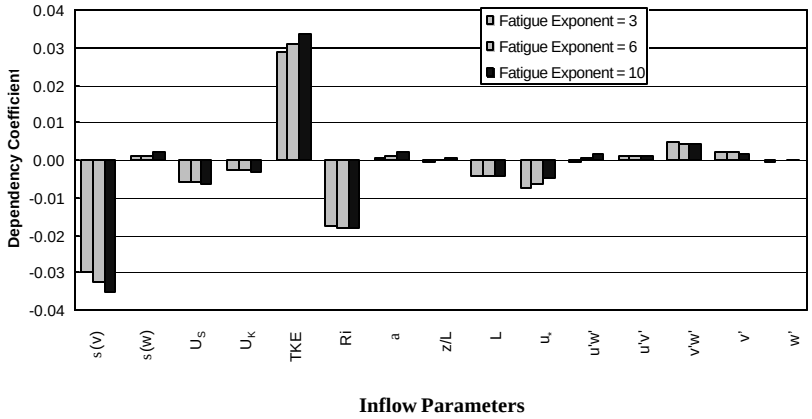

Fig. 11b. Wind Speed Class 7.

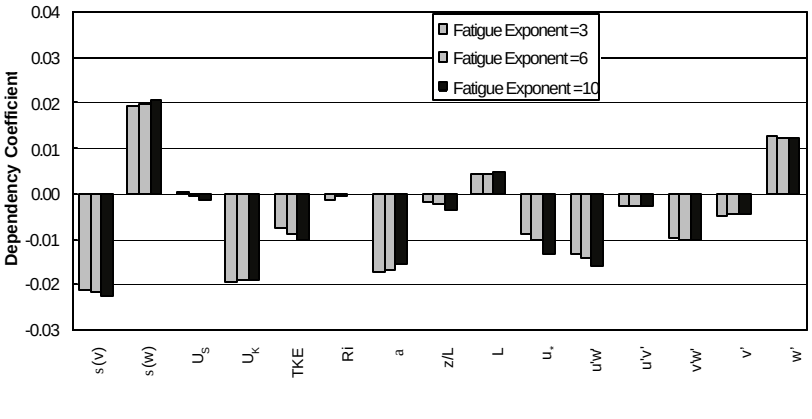

Fig. 11c. Wind Speed Class 8.

Fig. 11. Dependence Coefficient for Flap Bending by Wind Speed Class.

techniques to correlate the entire population (unstratified) inflow turbulence properties with the slope of the high-loading tail (cycle frequencies less than 100/h) of the alternating load spectra from two Micon 65 turbines operating side-by-side. In this analysis, the observed variance of the root flap bending loads was explained mainly by the variations in the hub-height friction velocity, u_*; the variance of the root edge bending moment was explained mainly by the friction velocity, u_* and the Reynolds stress component, $v'w'$; and the variance of the low-speed shaft torque, which is directly proportional to power, was explained mainly by the hub-height (local) friction velocity, u_*, and the *dynamic* stability of the atmospheric layer occupied by the wind turbine expressed by the gradient Richardson number, *Ri*. Thus lateral and vertical turbulence characteristics are associated with load variance on wind turbines.

The other two studies used multi-variable regression techniques. These techniques were used to access the dependence of the damage contained in the root bending spectra, as exemplified by the equivalent fatigue load in bending, to various inflow parameters. Both analyses were stratified by wind speed class; namely, the correlation between the inflow parameters and the fatigue load was studied over relatively small bands (bins) of the mean wind speed. The general conclusion from these studies is that the vertical and lateral turbulence components of wind speed have the highest correlation to the blade fatigue loads. The study by Sutherland [8,9] also

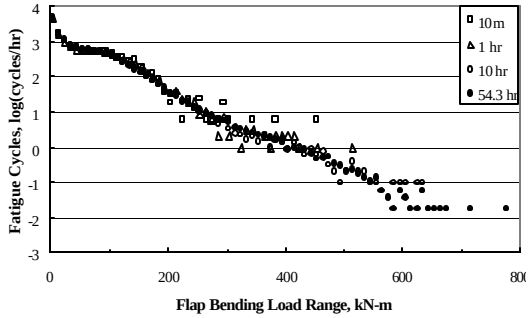

Fig. 12a. Flapwise Bending.

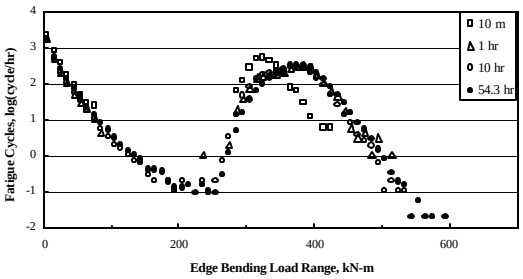

Fig. 12b. Edgewise Bending.

Fig. 12. Fatigue Spectra for Class 6 Wind Speeds.

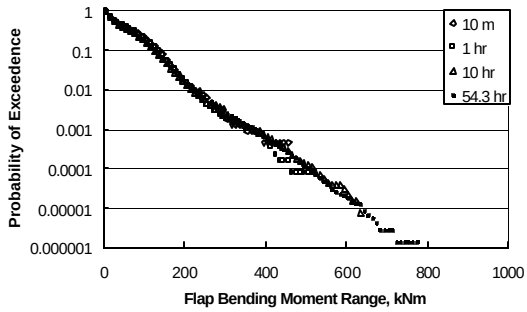

Fig. 13a. Flapise Bending.

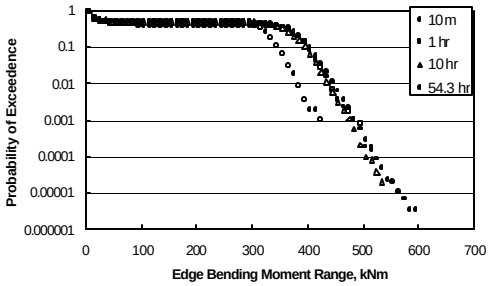

Fig. 13b. Edgewise Bending.

Fig. 13. Fatigue Spectra for Class 6 Wind Speeds.

included the dynamic stability parameter or gradient Richardson number, *Ri*, in the analysis. This parameter also had a relatively high correlation to the blade fatigue loads.

Dependence of Inflow Parameters

The results of multi-variable dependence analysis are shown in Fig. 10. As shown in this figure, the highest dependency of the fatigue loads on inflow parameters is for the standard deviation of the vertical component of the inflow, *s(w')* and the turbulence kinetic energy, *TKE* contained in the inflow.

For the other classes of wind speeds, see Fig. 11 for the analysis of flapwise fatigue in wind speed classes 5, 7 and 8, the dependency shifts between these inflow parameters and several others. In particular, the standard deviation of the cross-rotor component of the inflow, *s(v')* is also important. For flapwise bending, the *s(v')* and *s(w')* appear to be the most important across all wind speed classes examined here. This is also true for edgewise bending, but the *TKE* also has high dependence coefficients.

FATIGUE LOAD SPECTRA

One of the objectives of the LIST program is to obtain long-term fatigue spectra for the turbine blade loads. The 445 fatigue spectra for 10-minute records in wind class 5 offer an important database for studying long-term fatigue spectra.

Representative fatigue spectra are shown in Figs. 9 and 12. Exceedance diagrams for the spectra shown in Fig. 12 are shown in Fig. 13. In these two figures, the fatigue spectra are typical for this class of turbines. Namely, the edge-bending spectra display a bi-modal distribution, see Figs. 12b and 13b, that is directly attributed to the large 1P gravity component of the bending moment, see Fig. 7. As illustrated in Figs. 12b and 13b, the fatigue spectrum for flap-bending moment has a very different character, with a single-mode distribution.

Figures 12 and 13 illustrate the effect of increasing the length of the data records. In particular, the floor of the distribution continued to decrease from to 1 cycle in 10

minutes, to 1 cycle in 1 hour, to 1 cycle in 10 hours, and, finally, to 1 cycle in 54.3 hours. The important implication in these data is that as the floor is lowered, the range of the highest fatigue cycles is increased. When Class 5 wind speeds are analyzed, with over 74 hours of data, the same observation is made. Thus, these data do not show a maximum range, and all indications are that the spectra continues to higher ranges, albeit with lower rates of occurrence.

These data also indicate that the extrapolation of relatively short-term spectra to long-term spectra is consistent with measured data. In particular, Fig. 13 illustrates that the shape of the exceedance curves are set by 10 hours of data but may not be with one hour of data.

LONG-TERM EXTREME LOADS

The extreme loads are one of the major drivers in the design of wind turbines. The data set examined here provides a statistical look at these events.

Madsen, Pierce and Buhl [14] and Laino and Pierce [15] have addressed the statistical uncertainty of loads prediction using structural dynamics simulation codes. The data presented here offer measured data that may be used to examine load extremes for the operating wind turbine.

The extreme load in each ten-minute data set for Class 6 wind speeds is shown in Fig. 14. For the entire set of flap bending loads, the mean value is 566 kNm with a standard deviation of 37 kNm; i.e., a covariance (ratio of the standard deviation to the mean) of 6.5 percent. For the high flap moment data (< 590 kNm), these values are 618 kNm, 23 kNm, and 3.7 percent, respectively. For the edge bending loads, these values are 291 kNm, 16 kNm, 5.4 percent for the entire data set and 315 kNm, 7.9 kNm, and 2.5 percent for the high edge moment data (< 300 kNm), respectively.

Following the lead of Refs. 14 and 15, the distribution of the measured, maximum bending-moment from each ten-minute record was fit with a Gumbel distribution, as shown in Fig. 14. When the entire data set is considered in the fitting process, the Gumbel distribution does not track the high moment data. However, when only the high end of the measured distribution is considered, then the fit is significantly better. Similar comparisons were obtained for the other wind speed classes.

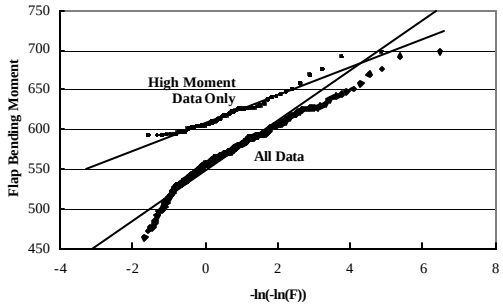

Fig. 14a. Flapwise Bending.

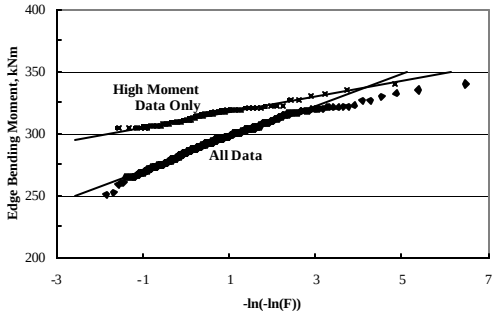

Fig. 14b. Edgewise Bending.

Fig. 14. Gumbel Distribution of the Load Extremes for Bin Class 5 Wind Speeds.

CONCLUDING REMARKS

The long-term data set from the ART has been used to collect another data set for the LIST program. This data set is from an upwind, two-bladed teetered-hub turbine located downwind of mountainous terrain. This data set is in sharp contrast to the initial data that examined the response of a 3-blade, upwind turbine at a typical Great Plains site. The data from this measurement campaign was used to examine the structural response of the ART. Both short and long term loads were examined. The correlation between inflow parameters and fatigue loads was quantified. Long term fatigue spectra were presented, and the distribution of extreme loads was examined. The analysis of inflow parameters and equivalent fatigue loads illustrate that the vertical and cross-rotor component of inflow velocity and the total kinetic energy consistently have the most influence on the fatigue spectrum. Long-term fatigue spectra illustrate that extrapolations of relatively short-term data are consistent with long-term measured data. Extreme operational loads are characterized using Gumbel distributions. While the Gumbel distribution did not

track the entire measured distribution, this distribution did track the high end of the bending moment distribution very well.

REFERENCES

1. Snow, A.L., Heberling, C.F., II, and Van Bibber, 1989, L.E., *The Dynamic Response of a Westinghouse 600-kW Wind Turbine*, SERI/STR-217-3405, Solar Research Institute.

2. Hock, S.M., Hausfeld, T.E., and Thresher, R.W., 1987, *Preliminary Results from the Dynamic Response Testing of the Westinghouse 600-kW Wind Turbine*, SERI/TP-217-3276.

3. McCoy, T.J., Malcolm, D.J., and Griffin, D.A., 1999, *An Approach to the Development of Turbine Loads in Accordance with IEC 1400-1 and ISO 2394* ASME Wind Energy Symposium AIAA/ASME, pp. 1-9.

4. Malcolm, D.J., McCoy, T.J., 2000, "Results from the Advanced Research Turbine Project," *2000 ASME Wind Energy Symposium*, AIAA/ASME, pp. 277-286

5. Kelley, N., Hand, M., Larwood, S., and McKenna, E., 2002, "The NREL Large-Scale Turbine Inflow and Response Experiment – Preliminary Results," *2002 ASME Wind Energy Symposium*, AIAA/ASME, pp. 412-426.

6. Fragoulis, A.N., 1997, "The Complex Terrain Wind Environment and Its Effects on the Power Output and Loading of Wind Turbines," 1997 ASME Wind Energy Symposium, AIAA/ASME, pp. 33-40.

7. Mounturb Final Report, 1996, G. Glinou and A. Fragoulis, eds., 3 vols., JOU2-CT93-0378.

8. Sutherland, H.J., 2002, "Analysis of the Structural and Inflow Data from the LIST Turbine," JSEE, in publication.

9. Sutherland, H., 2002, *Inflow and the Fatigue of the LIST Wind Turbine*, 2002 ASME Wind Energy Symposium, AIAA/ASME, pp. 427-437.

10. Rohatgi, J.S., and V. Nelson, 1994, *Wind Characteristics, An Analysis for the Generation of Wind Power*, Alternative Energy Institute, Canyon, TX, 237 p.

11. Kelley, N.D., and H.E. McKenna, 1996, "The Evaluation of a Turbulent Loads Characterization System." *1996 ASME Wind Energy Symposium*, AIAA/ASME, pp. 69-77.

12. Kelley, N.D., A.D. Wright, M.L. Buhl, Jr., and J.L. Tangler, 1997, "Long-Term Simulation of Turbulence-Induced Loads Using the SNL WINd-3D, FAST, YawDyn, and ADAMS Numerical Codes," *1997 ASME Wind Energy Symposium*, AIAA/ASME, pp. 74-85.

13. Kelley, N.D., "The Identification of Inflow Fluid Dynamics Parameters that can be Used to Scale Fatigue Loading Spectra of Wind Turbine Structural Components," *1994 ASME Wind Energy Symposium*, AIAA/ASME, pp. 181-196.

14. Madsen, P.H., K. Pierce and M. Buhl, 1999, "Predicting Ultimate Loads for Wind Turbine Design," *1999 ASME Wind Energy Symposium*, AIAA/ASME, T. Ashwill, ed., p. 355.

15. Laino, D.J., and K.G. Pierce, 2000, "Evaluating Statistical Loads Extrapolation Methods," *2000 ASME Wind Energy Symposium*, AIAA/ASME, P. Migliore, ed., p. 424.

APPENDIX: NOMENCLATURE

$\overline{U(z)}$ = mean horizontal wind speed at height z, m/s

z = height above ground, m

$\overline{u'}, \overline{v'}, \overline{w'}$ = mean, streamwise, crosswind, and vertical instantaneous turbulent eddy wind component velocities in a right-handed coordinate system where the longitudinal or streamwise wind component is parallel to the mean streamline, m/s

$\overline{u'w'}, \overline{v'w'}, \overline{u'v'}$ = mean turbulent Reynolds stress components, $(m/s)^2$

u_* = hub-height (local) friction velocity, m/s

$$\sqrt{\left|\overline{u'w'}\right|}$$

Ri = gradient Richardson number,

$$\left(g/\overline{q_m}\right)\left(\Delta\overline{q(z)}/\Delta z\right) \Big/ \left(\Delta\overline{U(z)}/\Delta z\right)^2$$

g = gravity acceleration, m/s^2

D = difference between measurements at 3 and 61 m

$\overline{q(z)}$ = mean potential temperature at height z, K

$$\overline{T(z)}\left[1000/\overline{P(z)}\right]^{0.286}$$

$\overline{T(z)}$ = mean absolute virtual temperature (corrected for effects of moisture) at height z, K

$\overline{P(z)}$ = mean local atmospheric pressure at height z, hPa

$\overline{q_m}$ = layer (61m to 3m) mean potential temperature, K

a = vertical wind shear exponent across rotor, where subscripts represent height above ground,

$$\frac{\overline{U_{58}}}{\overline{U_{15}}} = \left(\frac{z_{58}}{z_{15}}\right)^a$$

L = Obukhov scaling length, m

$$\frac{-\overline{\theta_s}\, u_*^3}{0.4\, g\, \overline{\left(w'\, \theta_s'\right)}}$$

$\overline{q_s}$ = mean potential temperature from sonic anemometer at hub height, K

$q_s'(t)$ = instantaneous potential temperature from sonic anemometer at hub height, K

$$q_s(t) - \overline{q_s}$$

TKE = turbulence kinetic energy, (m/s)^2

$$1/2\left[(u')^2 + (v')^2 + (w')^2\right]$$

σ(v') = standard deviation of v' (similar for w')

$$\sqrt{\frac{1}{N}\sum_{i=1}^{N}\left[v_i'\right]^2}$$

U_S = skewness coefficient of hub-height horizontal wind speed

$$\frac{1}{N}\sum_{i=1}^{N}\left[U_i(t) - \overline{U}\right]^3 \Big/ \frac{1}{N}\sum_{i=1}^{N}\left[U_i(t) - \overline{U}\right]^2$$

U_K = normalized kurtosis coefficient of hub-height horizontal wind speed

$$\frac{1}{N}\sum_{i=1}^{N}\left[U_i(t) - \overline{U}\right]^4 \Big/ \frac{1}{N}\sum_{i=1}^{N}\left[U_i(t) - \overline{U}\right]^2$$

t = individual samples at 40 Hz

N = 24000 samples per 10-minute record